Monroy Lafuente, L., Magnus, J., González Herráez, M., Naranjo Vega, F.B. & Kieu, K. 2023, "Numerical evaluation of spectral coverage and spectral resolution in coherent Raman scattering spectroscopy using a broadband fiber laser source", Journal of Raman Spectroscopy, vol. 54, no. 9, pp. 1001-1010.

Available at https://doi.org/10.1002/jrs.6579

Monroy Laura (Orcid ID: 0000-0002-1764-2267)
Joshua Magnus (Orcid ID: 0009-0009-0409-006X)

Numerical evaluation of spectral coverage and spectral resolution in coherent Raman scattering spectroscopy using a broadband fiber laser source

L. Monroy[1*], J. Magnus[2], M. González-Herráez[1], F. B. Naranjo[1], K. Kieu[2]

[1]Grupo de Ingeniería Fotónica, Dept. Electrónica (EPS) Universidad de Alcalá, Campus Universitario Alcalá de Henares 28871, Madrid, Spain
[2]James C. Wyant College of Optical Sciences, The University of Arizona, 1630 E. University Blvd., Tucson, Arizona 85712, USA
*Corresponding author: laura.monroy@uah.es

Abstract

We theoretically investigate the feasibility of using a fiber laser source for high resolution and broadband coherent Raman scattering (CRS) spectroscopy/imaging employing spectral focusing technique. To accomplish this task, we have developed a simulation tool where the laser pulse parameters can be imported directly from any pulse propagation software using split-step Fourier method to evaluate the spectral resolution and spectral coverage of CRS spectroscopy. Thus, the simulation tool can accommodate optical pulses of arbitrary shape and central wavelength, being also a user-friendly and versatile open-source software. We validate the numerical simulation tool by comparing its results with published theoretical and experimental data. We then use the tool to study the feasibility of using an all-fiber laser source for high resolution CRS spectroscopy in both the C-H window and the fingerprint region. This tool has a broad scope of applications in multiple fields where CRS spectroscopy is useful such as biomedicine, materials characterization, and biological imaging.

Keywords: CRS spectroscopy, simulation tool, spectral focusing, spectral resolution

1. Introduction

In the last decade, coherent Raman scattering (CRS) which includes stimulated Raman scattering (SRS) and coherent anti-Stokes Raman scattering (CARS) has emerged as the most recognized method of vibrational spectroscopy and microscopy [1,2]. CRS has become a widely used technique in several applications, such as biomedical imaging [3-5] and in material sciences as a characterization tool [6,7] among others, owing to its inherent properties including non-invasiveness, high sensitivity, three-dimensional imaging capability and chemical identification of samples or living cells without the use of fluorescent dyes or labels [8,9]. CARS is based on a four-wave mixing process [10] – a shorter wavelength pulse, namely the pump with angular frequency ω_p interact with a longer wavelength, the Stokes beam, with angular frequency ω_S, in a nonlinear material, resulting in an anti-Stokes signal (AS) with a frequency of $\omega_{AS} = 2\omega_p - \omega_S$, blue-shifted with respect to the input wavelengths. On the other hand, the SRS signal appears at the same wavelength as the excitation fields, in which the Stokes beam experiences a gain in intensity, namely stimulated Raman gain (SRG), while the pump experiences an intensity loss (SRL). In CARS, the AS signal is resonantly enhanced when the difference of the pump and Stokes frequencies matches a Raman resonance in the sample under study $(\omega_R = \omega_p - \omega_S)$. This implies that by using broadband sources in combination with a high

resolution and high-speed scanning mechanisms, multiple vibrational transitions in a sample can be interrogated. These properties make CARS and SRS a powerful intrinsic label-free imaging/spectroscopy tool for chemical identification of a wide variety of compounds. [11-15].

Nevertheless, the main drawback of most CRS spectroscopy/imaging systems is their complexity. Both CARS and SRS require a synchronized interaction of the two different laser pulses within the sample (in time, space and polarization). Additionally, the wavelengths of these pulses must be tunable over a wide range to cover the vibrational frequencies of the molecules of interest (mainly in the fingerprint and C-H window regions). Solid state lasers based on Ti:sapphire or Nd:YVO_4 crystals have been successfully used to perform CRS spectroscopy/imaging [16-18]. However, they are still very expensive, bulky and difficult to use [19]. For that reason, a strong push to develop compact, low-cost laser sources based on optical fiber format has been taking place [20]. As the result, various fiber laser sources have been demonstrated to be suitable for CARS and SRS spectroscopy/imaging in various capacity [20-25]. Notable results have been published with fiber based optical parametric oscillator approach [26-28], where the full fingerprint window is covered. However, it is still difficult to scale up the power output of these fiber laser systems to meet the demand of most practical applications with low-cost configurations. The main reason is the use of narrow band transform-limited picosecond pulses for both the pump and Stokes beams.

On the other hand, broadband fiber laser sources have a great potential for output power scaling using chirped pulse amplification technique (CPA) [27]. It turns out that high resolution CARS and SRS spectroscopy can be realized by broadband sources where the laser pulses are chirped instead of being transform-limited [29,30]. This principle is known as the spectral focusing technique (SF) [29-36]. An optimization of the CRS system can be accomplished by chirp-matching the pump and Stokes pulses, that is, both beams must have identical chirp rate. One of the simplest chirp control techniques can be accomplished by using a variety of passive optical elements such as optical fibers, prisms [37,38], spatial modulators [39,40], or dispersion gratings [27], among others.

The two main parameters that determine the viability of a CRS system for most practical application are the spectral resolution and the spectral coverage. The spectral resolution in SF-CRS systems is defined as the ability to distinguish two closely located resonances. The spectral resolution can be calculated as the bandwidth of the cross correlation between the pump and Stokes pulses, represented as $I_p(t)I_S^*(t)$, being I_p the intensity of the pump beam and I_s the Stokes intensity. This spectral resolution is mainly limited by the chirp rates as well as by the similarity of these chirps [41,42]. On the other hand, the difference between the frequency components of the pump and Stokes electric fields, also known as the instantaneous frequency difference (IFD), and denoted from this point as Ω, corresponds to a single Raman resonance (ω_R) [43,44]. Each of the Raman frequencies can be probed by introducing a time delay varying the temporal overlap of the pump and Stokes pulses [45]. Thus, high-speed scanning of the time delay allows for the acquisition of spectral resonances in a short period of time. Therefore, the Raman signal ω_R and its 1/e bandwidth $\Delta\omega_R$ determine the Raman mode and the spectral resolution, respectively. The schematic representation of the time-overlapping of two Gaussian pump (higher frequency) and Stokes (lower frequency) pulses at three different time delays is shown in Fig. 1(a). As it can be seen in this figure, the IFD value decreases ($\Omega_c < \Omega_b < \Omega_a$) as the time delay increases (positive delay). On the other hand, if the Stokes beam arrives before the pump (negative delay), the IFD value becomes larger as a function of delay time. Therefore, the optical bandwidth denoted by the maximum and minimum IFD values will be related to the spectral coverage as explained in the following section. The out-of-resonance frequencies related to the interactions involving the highly detuned electronic energy levels become part of the background noise. However, the background noise can be eliminated by multiple techniques such as polarization-sensitive detection [46], Epi-CARS spectroscopy [47], or frequency modulation CARS [48]. In these cases, a pulse-shaping approach has been incorporated so that

only a portion of the pump and Stokes pulses overlap in time. This method is based on the restriction of the excitation overlapping portion, plotted in Fig. 1(a) with green-dashed lines, not only enables the suppression of the non-resonant background noise, but also gives a high spectral resolution [49].

When the chirp of the pump and Stokes pulses are matched, the IFD value remains constant along the pulse overlapping at each time delay. This can be easily confirmed by comparing the slope (chirp-rate) of both pulses in the time-frequency representation (spectrogram) of Fig. 1(a). As the time delay increases (as one of the pulses is delayed in time relative to the other pulse), different IFD values of the chirp-matched pulses are obtained. Furthermore, the intensity of the Raman signal, whose bandwidth is related to the spectral resolution, will vary as a function of the time delay, and is maximized when the two pulses are fully overlapped. However, when nonlinear chirps are present in the optical pulses, the IFD is no longer constant but changes over the pulse duration. This results in a reduction of the Raman signal intensity (same IFD values but lower intensities at each time delay), which leads to the lessening of the spectral coverage and spectral resolution (the cross-correlation bandwidth of the Raman intensity signal depends on the chirp similarity) [41,44]. The same principle is accomplished when the pulses are not chirp-matched (different slopes imply different IFD value during the overlap of the pulses and less Raman signal intensity at the output). An example of the maximum spectral resolution (complete coincidence of the incident beams) of two linearly-chirped Gaussian pulses is shown in Fig. 1(b). The overlapping of the pump (blue line) and Stokes (orange dashed line) beams is represented on the inset of Fig. 1(b) at three different time delays.

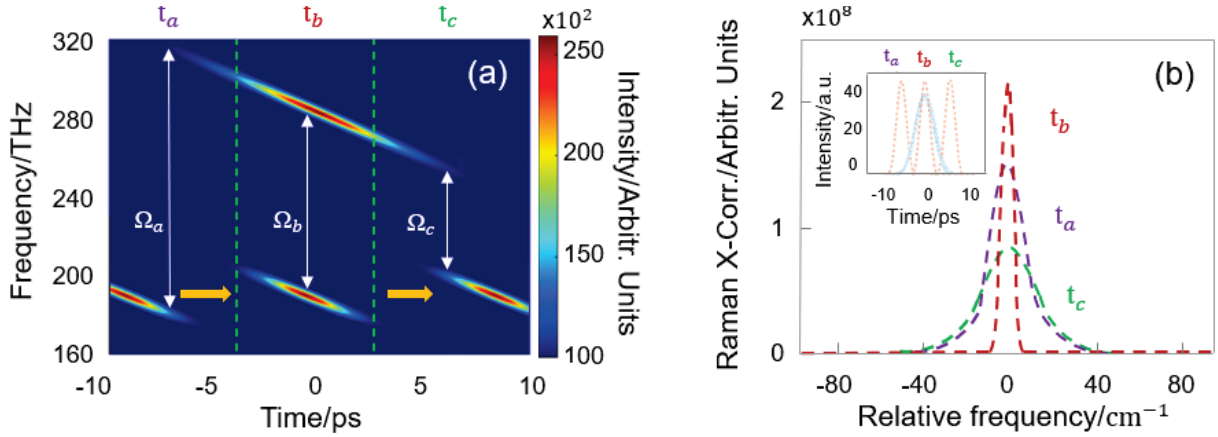

Fig 1. (a) Time-frequency representation of Gaussian ultrashort pump (higher frequency) and Stokes (lower frequency) pulses with linear chirp. Green-dashed line separates the interaction region for each shown time delay (t_a, t_b, t_c). (b) Spectral resolution calculation of the AS signal due to the cross-correlation of the pump and Stokes pulses at each time-delay (centered at 0 for simplicity). Inset: time-overlap of the pump (blue line) and Stokes (orange dashed line) Gaussian pulses at three different delays.

Spectral focusing is an established technique for high resolution and broadband CRS spectroscopy. However, it is still difficult to systematically describe the interaction between the pump and Stokes pulses that aren't exactly Gaussian, linearly chirped or perfectly chirp-matched. Based on the impact of the bandwidths/chirp rates of the pump and Stokes pulses on spectral resolution and coverage, we propose a numerical simulation approach for full characterization of a SF-CRS system using real pump and Stokes pulses as inputs. These input pulses are generated by solving the generalized nonlinear Schrödinger equation (GNLSE) considering both dispersive and nonlinear responses. The development of this Raman simulation tool allows researchers to connect the nonlinear pulse propagation simulation of their laser systems to the CRS spectral coverage and resolution (which has not been done before). This tool can be used to optimize and guide the design of ultrafast lasers. In this sense,

we provide a quantitative characterization tool for high resolution CRS spectroscopy experiments. This paper is organized as follows: first, a detailed description of the numerical simulation tool is given in Sec. 2. This incorporates the analysis of spectral coverage, spectral resolution, and the corresponding implementations in MATLAB. Then, Sec. 3 is where we validate our simulation tool by using published experimental data. We also investigate a practical scalable fiber laser system for SF-CRS spectroscopy working in both fingerprint and lipid region.

2. Simulation code and experimental validation

Throughout the work we assume that the CRS signal is generated by two ultrafast optical pulses, the pump and Stokes with the same input polarization and different central frequencies. The procedure, shown in Fig. 2, can be listed as follows: (i) the pump and Stokes beams are plotted in a time-frequency representation (spectrogram) to check the chirp-matching conditions and possible nonlinear effects on the pulse shape that could be detrimental for the spectral coverage and spectral resolution of the experiment [39,50]. (ii) The IFD values between the two pulses at each time delay are then determined, and the corresponding intensities of the Raman signal over the duration of the temporal overlap are calculated (CRS signal). (iii) Finally, the spectral coverage and spectral resolution are obtained at each time delay following the procedure explained in the previous section. This tool estimates the resolution and spectral coverage of the SF-CRS system, giving practical information as well as its limitations.

First, the pump and Stokes pulses are simulated using a pulse propagation simulation software based on the GNLSE equation. The complex amplitudes returned by these simulations are then used as the input for our MATLAB simulation tool.

A time-frequency representation (spectrogram) is calculated by using these 1-by-n matrix complex amplitudes, being n the number of points, and a Gaussian gate function, where the width of the gate function was chosen to compromise the resolution of the spectrogram in both the temporal and frequency domains. Therefore, an intensity matrix is obtained from the spectrogram of each pulse.

Subsequently, we measure the IFD by comparing the spectrogram of the pump and Stokes pulses at each time delay. In order to keep computing time low, we do not use the full matrix representation of the pump and Stokes pulses. Instead, for each time 'column' of the spectrogram (matrix) the frequency point which has the highest intensity is selected for both pulses. This allows us to use the shape of the chirped pulses with two 1-by-n matrices, rather than two n-by-n matrices. The IFD value can therefore be calculated as the frequency difference of these 1-by-n matrices.

The intensity of the cross-correlation (R) between the pump and Stokes pulses (Raman signal) is also calculated. The bandwidth of the Raman signal $\Delta\omega_R$ is the 1/e bandwidth of this cross-correlation, which determines the spectral resolution. The corresponding equations and simulation steps have been included in Fig.2.

The pump and Stokes pulses are shifted in time relative to one another. Initially, the Stokes pulse is shifted in time such that only one of the points overlaps with the pump beam. From this pair of points, their frequency difference and their Raman intensity are calculated. The Raman excitation intensity value is found as $I_p {I_S}^2$. Next, we shift the Stokes pulse so two points overlap, and calculate the two pairs of frequency differences and Raman intensities. We can continue this process of shifting the Stokes beam in time through the whole-time delay.

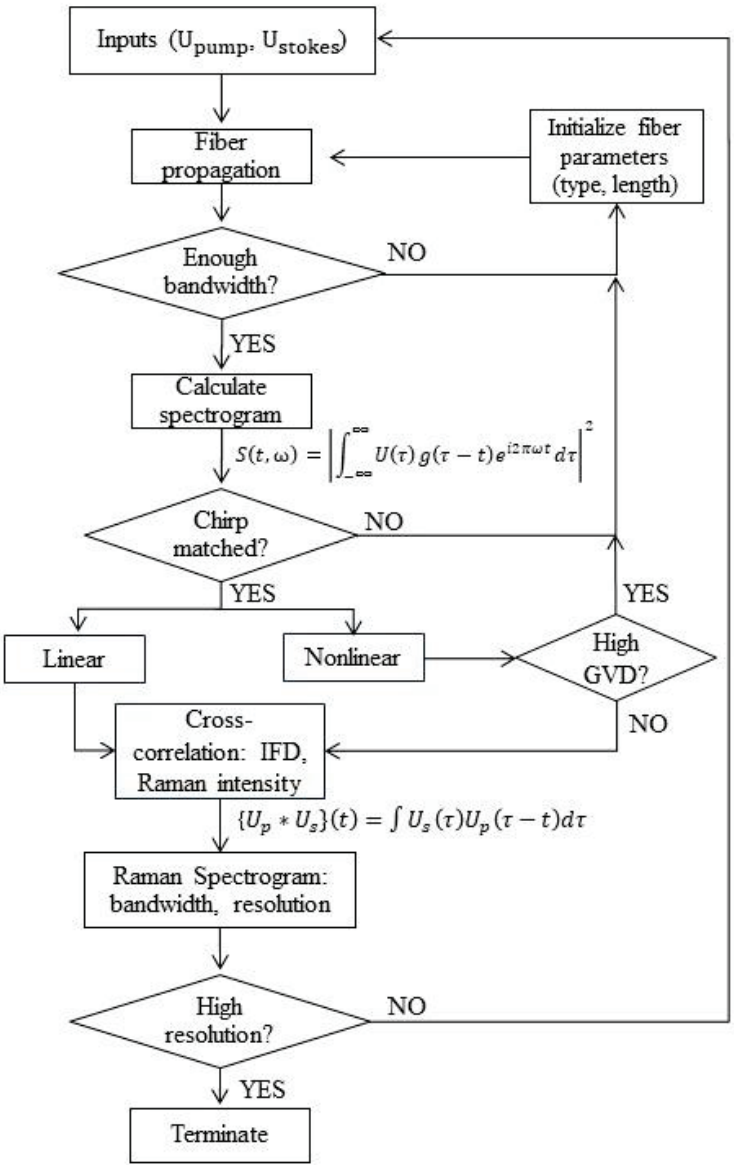

Fig. 2. Diagram of the Raman simulation algorithm for the estimation of the Raman spectral coverage and spectral resolution from nonlinear pulse propagation simulations. $U_s(t)$ and $U_p(t)$ are the electric field of the Stokes and pump pulses in the temporal domain, respectively.

After sweeping through the complete time delay, a matrix of IFD and Raman intensities is obtained for each time delay, whose size varies with the number of overlapping points. This n-by-n representation, which we have named the Raman spectrogram, is represented as a function of the time delay that was swept through on the x-axis, the y-axis is the frequency differences (IFD), and the z-axis (color coded) shows the weight of the Raman intensities of the calculated IFD at each time delay. The simulation procedure with the corresponding steps for the IFD and intensity calculations is shown in Fig. 3(a). In this case, the pump beam has a frequency of $\nu_p = 288.3$THz ($\lambda = 1040$ nm), whereas the Stokes beam is centered at $\nu_p = 193.4$ THz $\lambda = 1550$ nm). An example of a Raman Spectrogram is shown in Fig. 3(b). We define the spectral coverage as the spectral bandwidth at the 1/e maximum intensity decay of the Raman spectrogram, as represented in Fig. 3(b) with an orange and green line, respectively. The spectral resolution is calculated as the minimum value of the 1-by-n vector related to the 1/e bandwidth calculation of the cross-correlation of the pump and Stokes beams. A plot of spectral resolution versus time delay can be extracted from this calculation.

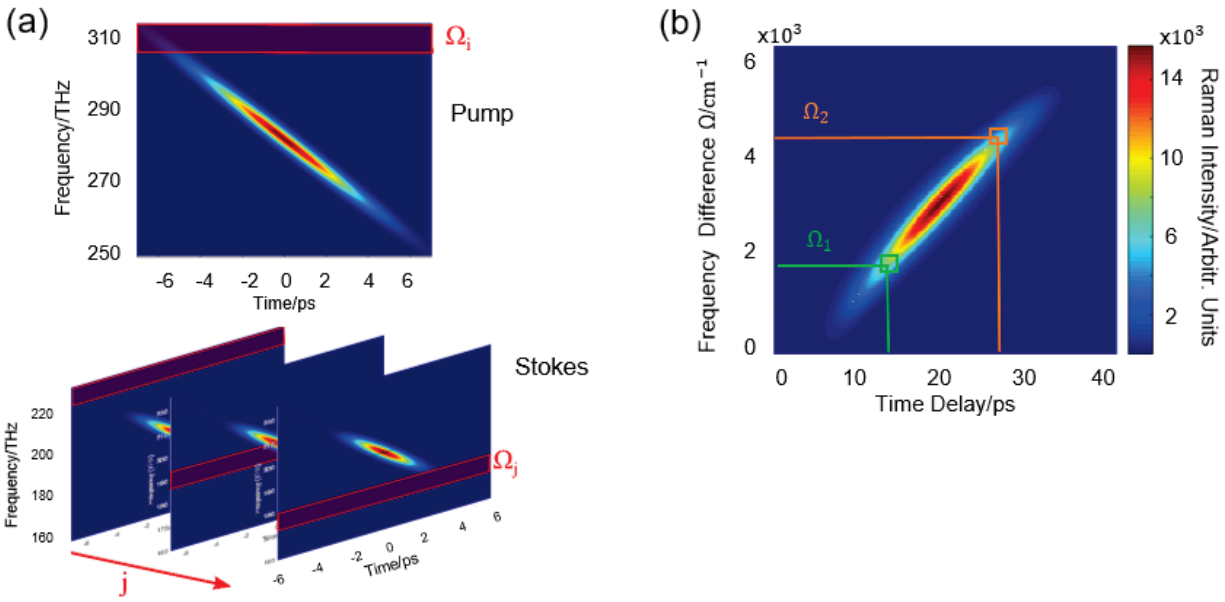

Fig. 3. Schematic procedure of the MATLAB simulation code (a) Calculation of the IFD from the pump and Stokes pulses at each time delay. (b) Calculation of the Raman spectrogram by the analysis of the intensity of the anti-Stokes signal as a function of the IFD and the relative time delay. The intensity values are collected by clusters and represented in a color bar function.

This simulation tool can accommodate optical pulses of arbitrary shape and central wavelength, making it a user-friendly and versatile open-source software. The suitability of the CRS system (pump and Stokes pulses generation) will be evaluated based on the estimation of the spectral resolution and spectral coverage by taking into account the values of the optical bandwidths and chirp values (chirp matching condition).

We validate the accuracy of our simulation tool by comparing our calculation results with published experimental results, published in [50]. In this example, a CRS signal centered at 3000 cm^{-1} (Fig. 4(a)) is simulated by calculating the cross-correlation of the pump and Stokes pulses. The spectral resolution calculation for each time delay is depicted in Fig. 4(b). Finally, we estimate the intensity of the CRS signal, plotted in a Raman spectrogram (Fig. 4(c)) in terms of the IFD and the relative temporal delay. From this representation we can calculate the spectral coverage, denoted by green-dashed lines. In this sense, a spectral coverage in the lipid region of 2620-3450 cm^{-1} and a spectral resolution of 8 cm^{-1} have been estimated in the simulation code for the relative temporal delay region of 5-11 ps. These measurements are in quantitative agreement with those shown in [50] (spectral resolution of 8 cm^{-1} in the 2800-3100 cm^{-1} wavenumber window). Furthermore, the optical resolution of 8 cm^{-1} coincides with the theoretical approximation obtained from [41].

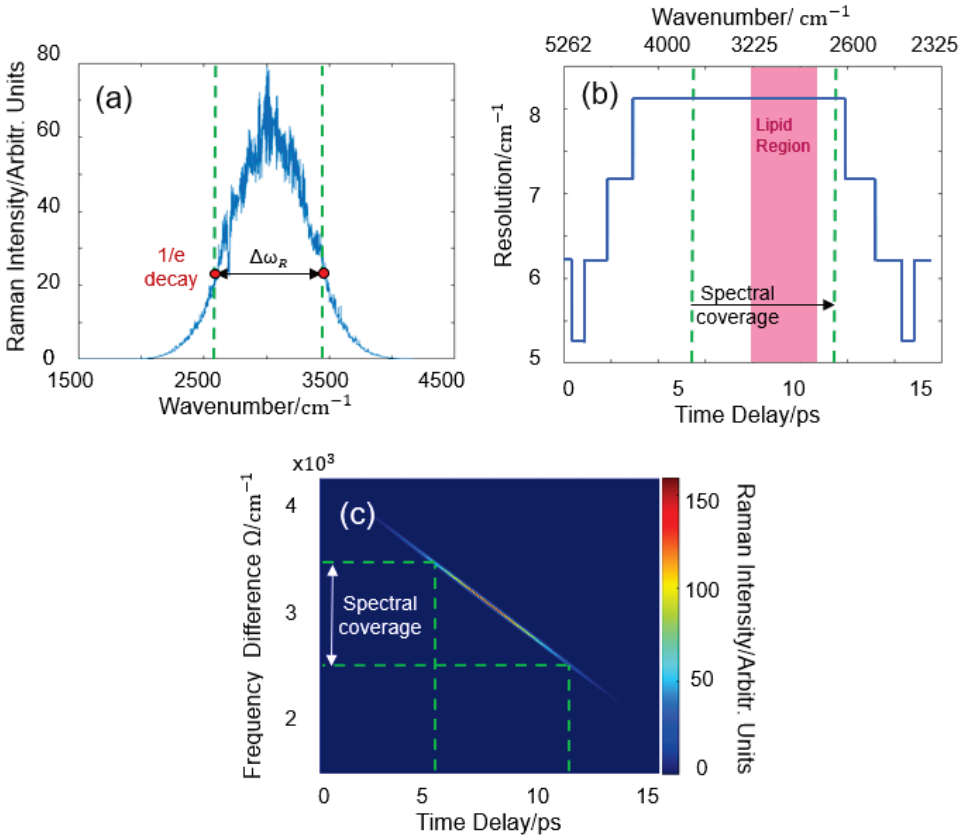

Figure 4. Simulation results of the experimental data from [50]. (a) CRS signal centered at 3000 cm^{-1} with a spectral coverage (measured as its FWHM) from 2600 to 3400 cm^{-1}, covering the lipid region. (b) Raman spectrogram of the experimental Gaussian pulses. (c) Spectral resolution from the cross-correlation function of the pump and Stokes pulses. The mean value of the spectral resolution in the region of coincidence is 8.1 cm^{-1}.

3. Proposal for Scalable All-Fiber Format Laser for CRS spectroscopy in both Fingerprint & Lipid Regions

As it was mentioned before, most CRS systems have a limited spectral coverage due to the use of narrow-band pump and Stokes pulses. This range can be expanded by employing tunable light sources, covering most of the vibrational frequencies of the molecules of interest, centered in the fingerprint and C-H window regions. However, the complexity, costs or issue with power scaling of these assemblies make it unfeasible to meet the demand of most practical applications. Here, we propose the development of a scalable all-fiber format source that can be used for CRS spectroscopy in the lipid and fingerprint regions simultaneously. The fiber laser source is based on our previous laser systems that have been developed in our laboratory. For that reason, we can perform our calculation using realistic physical parameters.

The laser cavity is based on a lab-built Er-doped fiber oscillator with a SWCNT-polymer composite for passive mode-locking operating at 100 MHz repetition rate [51,52]. The output ultrashort Gaussian laser pulse (centered at 1550 nm) is split by a 50/50 beam splitter into two arms to form the pump and Stokes beams. In order to generate the pump pulse, the laser pulse is sent through a high nonlinear fiber (HNLF, OFS) to generate a broadband supercontinuum (SC) spanning from 900 nm to 1800 nm [50]. Subsequently the region near 1040 nm of the SC is amplified using an Yb-doped fiber amplifier to create a high-power output pump beam. Both beams then travel through different lengths of fibers (single-mode fiber (SMF) and a single-clad fiber (SCF-UN-3, Coractive)), for chirp-matching purposes. A complete description of the fiber laser setup can be found in [51,53]. The schematic diagram of the fiber laser system for CRS

spectroscopy is plotted in Fig. 5. The nominal bandwidth of the 1040 nm source combined with the 1550 nm beam allows for spectral coverage in the lipid region [50].

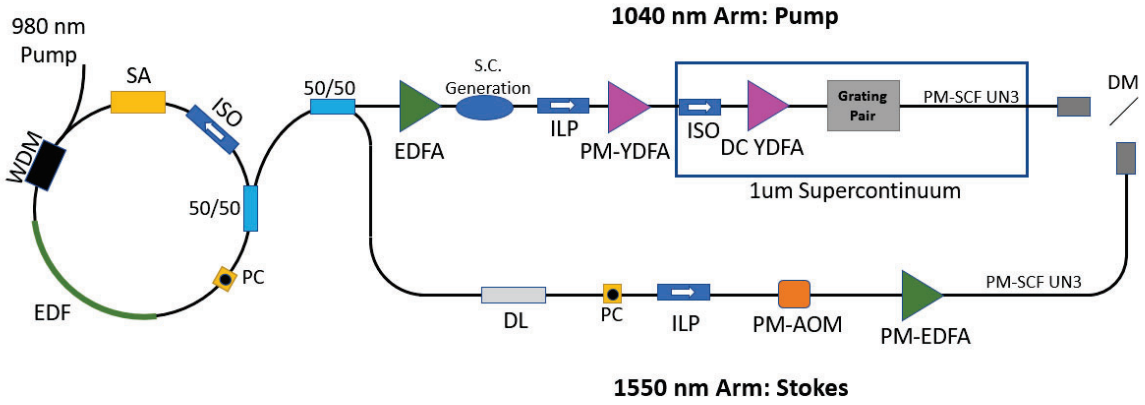

Fig. 5. Diagram of the fiber laser for CRS spectroscopy in both the fingerprint and lipid regions based on a passively mode-locked ring fiber laser cavity. WDM- wavelength division multiplexer; SA – saturable absorber; ISO – isolator; PC – polarization controller; EDFA – Er-doped fiber amplifier; SC – supercontinuum; ILP – In-line polarizer; PM-YDFA – Polarization maintaining Yb-doped fiber amplifier; DC-YDFA – Double-Clad YDFA; DM – Dichroic Mirror; DL – Delay Line; PM-AOM – Polarization maintaining acousto-optic modulator.

Next, to reach the fingerprint region (400 cm^{-1}-1600 cm^{-1}) we need two beams that are closer in central frequency to have spectral coverage at lower wavenumbers. To make spectral focusing technique to work, we need to make the 1040 nm signal stronger and wider (in spectrum domain), while also keeping the chirp rate almost linear. The laser system can be realized in fiber format, with the use of an intermediate grating pair for pulse compression in free-space. The alternative to the grating pair would be to use a hollow-core PCF for pulse compression, leading to a complete all-fiber format laser source. Subsequently, the 1040 nm pump pulse is separated into two sections by using a dichroic mirror centered at 1000 nm, creating a low-frequency beam, and a high-frequency beam. The combination of these three beams enables full spectral coverage in both the lipid and fingerprint regions. A schematic representation of the dual-coverage procedure is represented in Fig. 6.

To simulate the pump pulse, we explored different fibers and pulse parameters to generate a linearly-chirped SC pulse centered at 1040 nm. We used nonlinear pulse propagation using a split-step Fourier method for this purpose [54]. We found that an initial 10 nJ-Gaussian pulse can be compressed down to 100 fs using a free space grating pair. The pulse is then broadened self-similarly with parabolic shape by propagating through 1-m of PM-SCF-UN3 (Nufern). The broadened spectral bandwidth up to 300 nm in the spectral domain is achieved. The length of the SCF fiber, pulse compression and pulse energy have been optimized to maximize spectral broadening while keeping the chirp nearly linear. We have also simulated the pulse propagation of the 1550 nm Stokes beam accordingly to the chirp rate of the pump pulse in order to accomplish the chirp-matching condition of the SF-technique. The results of these pulse propagation simulations are shown in Fig. 7.

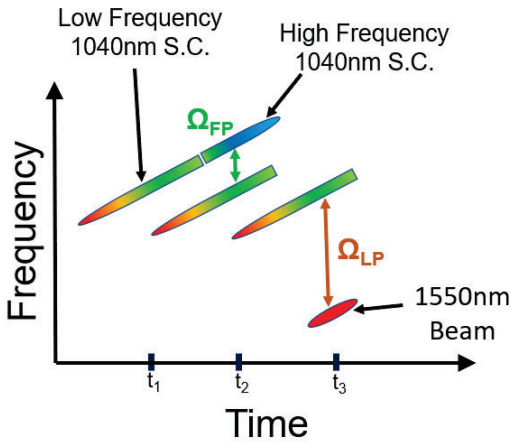

Fig. 6. Diagram of 'three beam method' for covering the fingerprint and lipid regions with the output of our laser system. The 1040 nm supercontinuum is split into two beams in free space, and the long wavelength side is put on a delay line and then overlaps in time with the short wavelength 1040 nm SC beam to excite the Raman resonances in the fingerprint region FP (600 cm^{-1} – 1600 cm^{-1}). The long wavelength can also overlaps in time with the 1550 nm beam to excite Raman resonances in the lipid region LP (2800 cm^{-1} – 3200 cm^{-1}).

Next, we make the connection from the GNLSE pulse propagation simulation to the Raman simulation to obtain the expected Raman spectral coverage and resolution. This connection between the pulse propagation simulation and the simulated Raman coverage and resolution can be a valuable tool for researchers using spectral focusing techniques for Raman spectroscopy. We have done two simulations, one for the lipid region and one for the fingerprint region. The lipid region uses the 1550 nm beam and the lower-frequency beam from the 1040 nm SC pump pulse. On the other hand, the fingerprint region simulation uses both sections from the 1040 nm SC pump pulse. We also implemented in the Raman simulation tool a method for simulating the dichroic mirror that splits the 1040 nm SC into two beams. This allows us to fully simulate the system, where the transition wavelength of the dichroic mirror is another degree of freedom. According to most common commercial dichroic mirrors, a split wavelength of 1000 nm has been set for this simulation.

The simulation results for the fingerprint region are shown in Fig. 8(a) and (b). A spectral coverage from 230 cm^{-1} to 1646 cm^{-1} is estimated, with an average resolution of ~13.4 cm^{-1}. Next, Fig. 8(c) and (d) show the simulation results for the lipid region. The estimated spectral coverage in the lipid region is from 1906 cm^{-1} to 3652 cm^{-1} with an average resolution of ~25.2 cm^{-1}. Both simulations show lower resolution than what would be expected from elementary calculations assuming perfectly linear chirps and Gaussian pulses (ideal case) [41]. The connection from the pulse propagation simulation to the Raman simulation allows for a first estimation of the system's resolution and the expected spectral range using real, non-ideal pulses. From the simulations we can determine that an all-fiber format laser system can be used for Raman spectroscopy to cover both the fingerprint region and the lipid region with high resolution simultaneously.

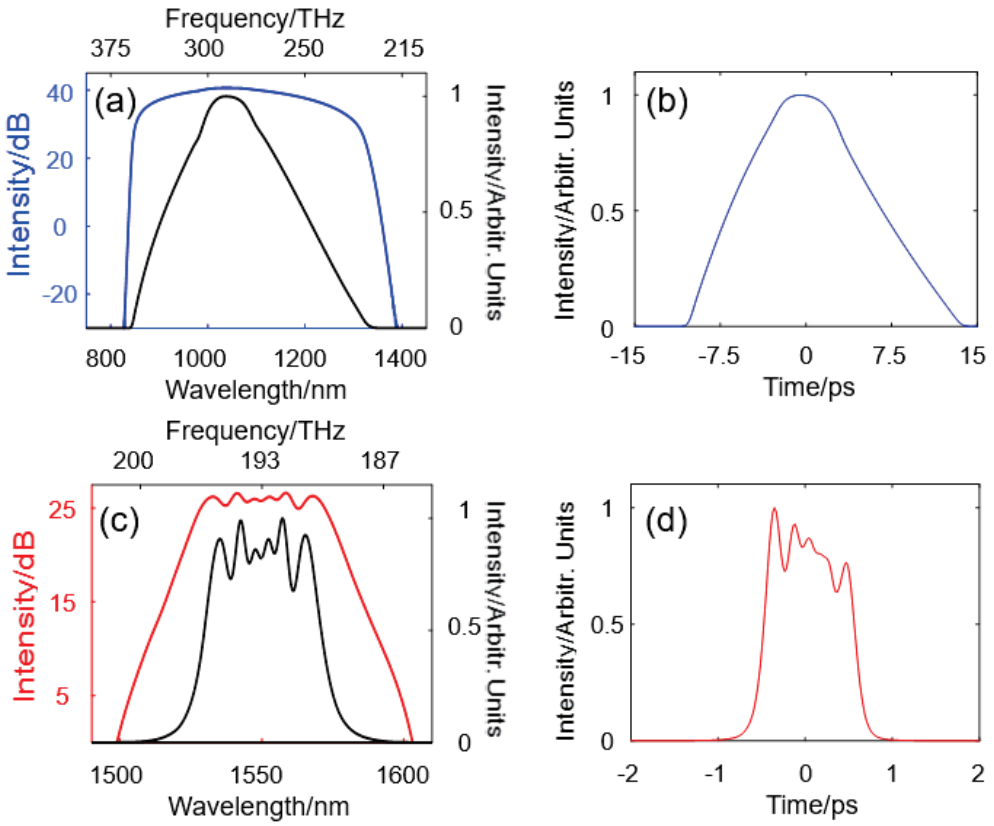

Fig. 7. GNLSE pulse propagation simulation results for chirp-matched 1550 nm (Stokes) and 1040 nm SC (pump) pulses. (a) Optical spectrum of the simulated SC 1040 nm pump pulse at the output of the fiber laser system in log scale (blue) and linear scale (black). (b) Temporal shape of the pump pulse after generating the SC and chirp compensation. (c) Simulated spectrum of the Stokes beam at the output of the laser system in log scale (red) and linear scale (black). (d) Temporal shape of the Stokes pulse.

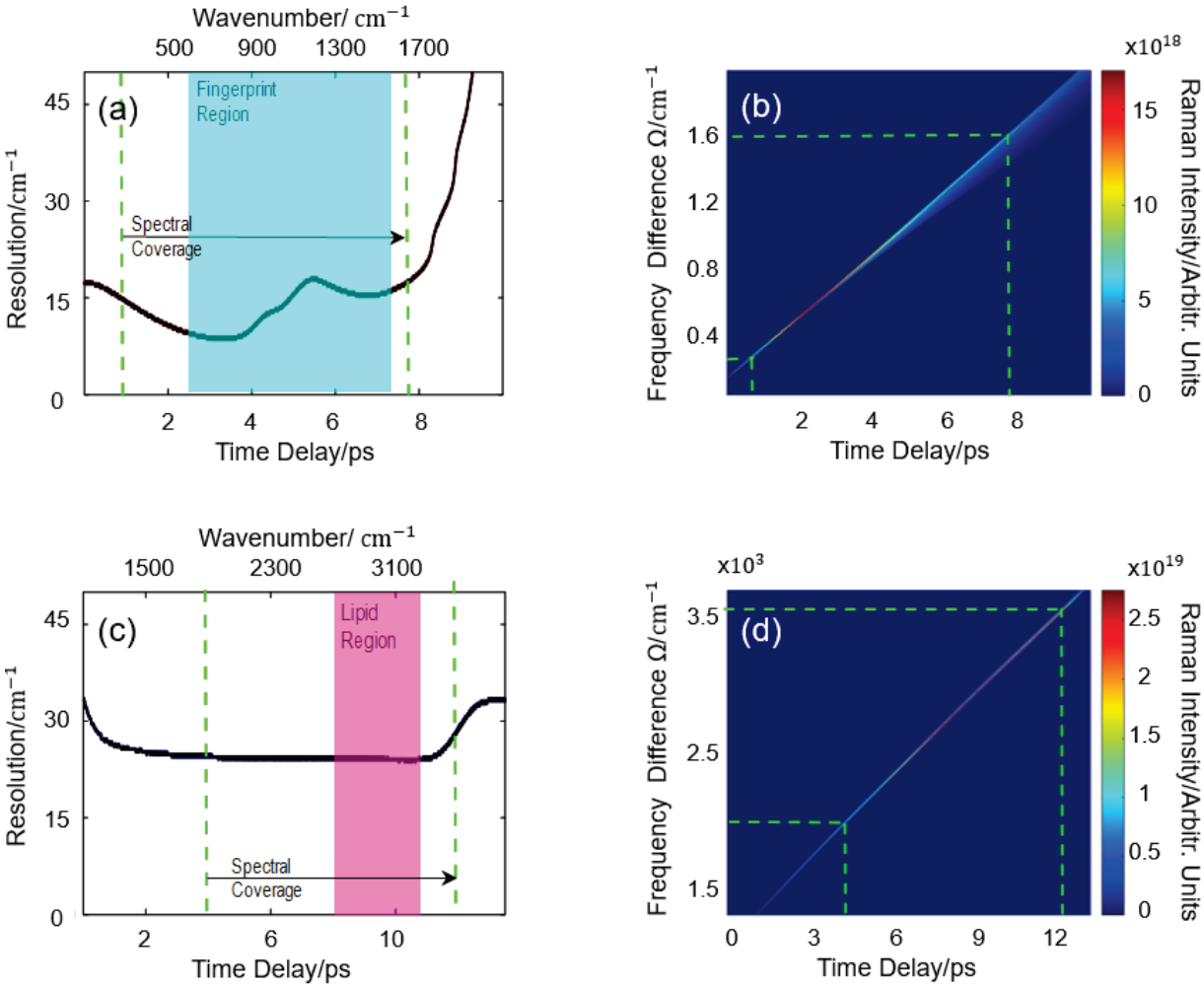

Fig. 8. Simulation results of the CRS dual-coverage spectroscopy all-fiber laser system (a) Spectral resolution of the coherent Raman signal in the fingerprint region with an average value of 13.4 cm^{-1}. (b) Raman spectrogram centered in the fingerprint region with a spectral coverage of 230 cm^{-1} to 1646 cm^{-1}. (c) Resolution calculation centered in the C-H window with an average value of 25.2 cm^{-1}. (d) Raman spectrogram for the C-H window with a spectral coverage ranging from 1906 cm^{-1} to 3652 cm^{-1}.

4. Summary and Conclusions

In summary, a novel simulation tool for spectral focusing CRS spectroscopy in both the fingerprint and lipid is presented. The tool is capable of modelling CRS signal in a wide variety of CRS geometries with arbitrary pulse shapes and energies. The influence of the laser pulse's chirp and pulse width on the CRS signal provides useful and critical information for the appropriate selection of the optical chirping device (PCF, HNLF, grating prisms, glass, etc.) in order to find the optimal working point of the CRS system. These results make this simulation code a useful tool in SF-CRS characterization due to its versatility and simplicity yet informative nature. We have also theoretically established that our scalable fiber laser system should be able to provide high resolution and full coverage of the fingerprint as well as the lipid windows. The experimental effort to build this laser system is currently underway. We expect the optics and photonics research community to adapt the open-source code-with respect to their specific experimental parameters and thus to benefit from the versatility of our simulation tool.

Acknowledgments. The authors thank Ruth Appleby for her support, and O. Batjargal for helpful comments. L. Monroy thanks Ministerio de Ciencia e Investigación for FPU grant.

Funding. Comunidad de Madrid (S2018/NMT-4326); Ministerio de Ciencia, Innovación y Universidades (RTI2018-097957-B-C31), Accelerate Diagnostics CARB-X (IDSEP160030).

References

1. C. W. Freudiger, W. Min, B. G. Saar, S. Lu, G. R. Holtom, C. He, J. C. Tsai, J. X. Kang, and X. S. Xie, *Science*, **2008**, vol. 322, no. 5909, pp. 1857–1861.
2. C. L. Evans and X. S. Xie, *Annu. Rev. Anal. Chem.* **2008**, vol. 1, pp. 883–909.
3. A. Fussell, E. Garbacik, H. Offerhaus, P. Kleinebudde, C. Strachan, *Eur. J. Pharm. Biopharm.* **2013**, *85*, 1141–1147.
4. T. Ideguchi, S. Holzner, B. Bernhardt, G. Guelachvili, N. Picqué, T. W. Hänsch *Nature* **2013**, *502*, 355–358.
5. C. L. Evans, E. O. Potma, M. Puoris'haag, D. Côté, C. P. Lin, X. S. Xie, *Proc. Natl. Acad. Sci. USA*, **2005**, *102(46)*, 16807-16812.
6. Y. Zhang, Y. R. Zhen, O. Neumann, J. K. Day, P. Nordlander, N. J. Halas, *Nat. Commun*. **2014**, *5*, 4424.
7. A. S. Duarte, J. Rehbinder, R. R. B. Correia, T. Buckup, M. Motzkus, *Nano Lett.* **2013**, *13*, 697.
8. J. Trägårdh, T. Pikálek, M. Šerý, T. Meyer, J. Popp, T. Čižmár, *Opt. Express* **2019**, *27*, 30055-30066.
9. C. W. Freudiger, W. Min, B. G. Saar, S. Lu, G. R. Holtom, C. He, J. C. Tsai, J. X. Kang, X. S. Xie, *Science* **2008**, *322*, 1857.
10. H. Lotem, R. T. Lynch, N. Bloembergen, *Phys. Rev. A* **1976**, *14*, 1748.
11. S. Michel, H. Rigneault, A. Courjaud, E. Mottay, C. Finot, J. M. Dudley, *J. Biomed. Opt.* **20011**, *16(2)*.
12. B. C. Chen, J. H. Sung, X. X. Wu, S. H. Lim*, J. Biomed. Opt.* **2011**, *16(2)*, 021112.
13. C. Camp Jr, Y. Lee, J. Heddleston, C. M. Hartshorn, A. R. H. Walker, J. N. Rich, J. D. Lathia, M. T. Cicerone, *Nature Photon* **2014**, *8*, 627–634.
14. T. Hellerer, C. Axäng, C. Brackmann, P. Hillertz, M. Pilon, A. Enejder, *Proceedings of the National Academy of Sciences* **2007**, *104(37)*, 14658-14663.
15. Y. Ozeki, W. Umemura, Y. Otsuka, S. Satoh, H. Hashimoto, K. Sumimura, N. Nishizawa, K. Fukui, K. Itoh *Nature Photon* **2012**, *6*, 845–851.
16. J. G. Porquez, A. D. Slepkov, *AIP Advances* **2018**, *8,* 095213.
17. K. J. Mohler, B. J. Bohn, M. Yan, G. Mélen, T. W. Hänsch, N. Picqué*, Opt. Lett.* **2017**, *42*, 318-321.
18. Y. Shen, A.A. Voronin, A.M. Zheltikov, S. P. O'Connor, V. V. Yakovlev, A. V. Sokolov, M. O. Scully, *Sci Rep* **2018**, *8*, 9526.
19. T.R. Monfort, **2018**, *PhD Thesis*, University of Southampton. Y
20. R. Selm, M. Winterhalder, A. Zumbusch, G. Krauss, T. Hanke, A. Sell, A. Leitenstorfer, *Opt. Lett.* **2010**, *35*, 3282-3284.
21. N. Coluccelli, C. R. Howle, K. McEwan, Y. Wang, T. Teddy Fernandez, A. Gambetta, P. Laporta, G. Galzerano, *Opt. Lett.* **2017**, *42*, 4683-4686.
22. C. W. Freudiger, W. Yang, G. R. Holtom, N. Peyghambarian, X. S. Xie, and K. Q. Kieu, *Nat. Photonics* **2014**, vol. 8, no. 2, pp. 153–159.
23. Y. Ozeki, T. Asai, J. Shou, and H. Yoshimi, *IEEE J. Sel. Top. Quantum Electron.* **2019**, 7100211
24. A. Gambetta, V. Kumar, G. Grancini, D. Polli, R. Ramponi, G. Cerullo, and M. Marangoni, *Opt. Lett.* **2010**, vol. 35, no. 2, p. 226.
25. B. Figueroa, W. Fu, T. Nguyen, K. Shin, B. Manifold, F. Wise, and D. Fu, *Biomed. Opt. Express* **2018**, *9*, 6116-6131.
26. M. Brinkmann, M. Brinkmann, M. Brinkmann, A. Fast, A. Fast, T. Hellwig, T. Hellwig, I. Pence, C. L. Evans, C. Fallnich, and C. Fallnich, *Biomed. Opt. Express*, **2019**, vol. 10, no. 9, pp. 4437–4449.
27. K. Yang, S. Zheng, Y. Wu, P. Ye, K. Huang, Q. Hao, and H. Zeng, Opt. Express **2018**, *26*, 17519-17528.
28. M. Baumgartl, M. Chemnitz, C. Jauregui, T. Meyer, B. Dietzek, J. Popp, J. Limpert, and A. Tünnermann, Opt. Express **2012**, *20*, 4484-4493.
29. R. Selm, M. Winterhalder, A. Zumbusch, G. Krauss, T. Hanke, A. Sell, and A. Leitenstorfer, Opt. Lett. **2010**, *35*, 3282-3284.
30. S. Karpf, M. Eibl, W. Wieser, T. Klein, and R. Huber, Nat Commun **2015**, *6*, 6784.
31. F. Röser, T. Eidam, J. Rothhardt, O. Schmidt, D. N. Schimpf, J. Limpert, and A. Tünnermann, *Opt. Lett.* **2007**, 32, 3495-3497.
32. T. Hellerer, A. M. Enejder, A. Zumbusch, *Appl. Phys. Lett.* **2004**, *85(1)*, 25–27.
33. W. Langbein, I. Rocha-Mendoza, P. Borri, *Appl. Phys. Lett.* **2009**, 95(8), 081109.
34. E. T. J. Nibbering, D. A. Wiersma, K. Duppen, *Phys. Rev. Lett.* **1992**, 68, 514.
35. E. Gershgoren, R. A. Bartels, J. T. Fourkas, R. Tobey, M. M. Murnane, H. C. Kapteyn, *Opt. Lett.* **2003**, *28*, 361-363.
36. K. Koike, N. I. Smith, and K. Fujita, Biomed. Opt. Express **2022**, *13*, 995-1004.

37. K. P. Herdzik, K. N. Bourdakos, P. B. Johnson, A. P. Lister, A. P. Pitera, C. Guo, P. Horak, D. J. Richardson, J. H. V. Price, S. Mahajan, *Appl. Phys. B* **2020**, *126(84)*.
38. I. Rocha-Mendoza, W. Langbein, P. Borri, *Appl. Phys. Lett.* **2008**, *93*.
39. L. Brückner, T. Buckup, M. Motzkus, *Opt. Lett.* **2015**, *40(22)*, 5204–5207.
40. L. Brückner, T. Buckup, M. Motzkus, *J. Opt. Soc. Am. B* **2016**, *33(7)*, 1482–1491.
41. R. A. Cole, A. D. Slepkov, *J. Opt. Soc. Am. B* **2018**, *35*, 842-850.
42. I. Rocha-Mendoza, W. Langbein, P. Borri, *J. Raman Spectrosc.* **2009**, *40*, 800–808.
43. Ji-Xin Cheng, Andreas Volkmer, X. Sunney Xie, *J. Opt. Soc. Am. B* **2002**, *19*, 1363-1375.
44. E. R. Andresen, P. Berto, H. Rigneault, *Opt. Lett.* **2011**, *36(13),* 2387-2389.
45. K. Chen, T. Wu, T. Chen, H. Wei, H. Yang, T. Zhou, Y. Li1, *Opt. Lett.* **2017**, *42(18)*, 3634-3637.
46. J. X. Cheng, L. D. Book, X. S. Xie, *Opt. Lett.* **2001**, *26*, 1341–1343.
47. J. X. Cheng, A. Volkmer, L. D. Book, X. S. Xie, *J. Phys. Chem. B* **2001**, *105*, 1277–1280.
48. C. L. Evans, X. S. Xie, *Annu. Rev. Anal. Chem.* **2008**, *1*, 883–909.
49. S. Postma, A. C. W. van Rhijn, J. P. Korterik, P. Gross, J. L. Herek, and H. L. Offerhaus, Opt. Express **2008**, *16(11)*, 7985–7996.
50. Y. Qin, B. Cromey, O. Batjargal, K. Kieu, *Opt. Lett.* **2021**, *46(1)*, 146-149.
51. K. Kieu, M. Mansuripur, *Opt. Lett.* **2007**, *32*, 2242.
52. K. Kieu, M. Mansuripur, *Opt. Lett.* **2008**, *33*, 64.
53. S. Mehravar, R. A. Norwood, N. Peyghambarian, K. Kieu, *Appl. Phys. Lett.* **2016**, *108*, 231104.
54. G. P. Agrawal, 3rd Edition, Academic Press, San Diego, **2001**.

Graphical abstract

The use of a numerical simulation tool enables us to evaluate the spectral resolution and spectral coverage of CRS spectroscopy. Preliminary results by using an all-fiber laser source for high resolution CRS spectroscopy in both the C-H window and the fingerprint region is presented. The simulation tool can accommodate optical pulses of arbitrary shape, being a user-friendly and versatile open-source software.

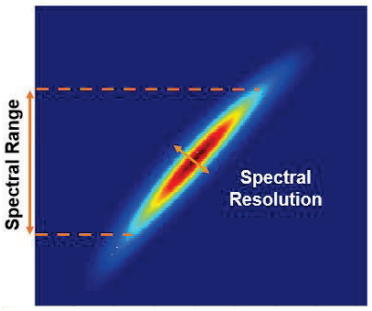

Numerical evaluation of spectral coverage and spectral resolution in coherent Raman scattering spectroscopy using a broadband fiber laser source

L. Monroy, J. Magnus, M. González, F. B. Naranjo and K. Kieu